54 COMPARISON OF 24 MAY 2011 GENESIS AND EVOLUTION OF SIMULATED MESOCYCLONES USING VARIOUS MICROPHYSICS SCHEMES WITH 1-KM GRID RESOLUTION

Derek Stratman[1,2] * and Keith Brewster[1]
[1]Center for Analysis and Prediction of Storms, Norman, Oklahoma
[2]School of Meteorology, University of Oklahoma, Norman, Oklahoma

1. INTRODUCTION

On the afternoon of 24 May 2011, an outbreak of twelve tornadoes, consisting of two EF-4 tornadoes and one EF-5 tornado, assailed northern and central Oklahoma within the Norman, OK, National Weather Service (NWS) Weather Forecast Office's county warning area. This outbreak caused 11 deaths and 293 injuries (see http://www.srh.noaa.gov/oun/?n=events-20110524 for more information). An extensive observation network was in place in this area during the spring of 2011, so despite the tragic loss of life, this is an ideal case to explore the Warn-on-Forecast (WoF) concept (Stensrud et al., 2009, 2013) with storm-scale numerical simulations.

The close proximity of the tornadic and non-tornadic supercells on this date made forecasting of storm tracks difficult for storm-scale models, but the Center for Analysis and Prediction of Storms (CAPS) real-time forecasting system had good success at simulating these storms. However, improvements in storm tracks might be expected using more sophisticated microphysics schemes or an ensemble of simulations with microphysics diversity. Therefore, the aim of this study is to examine the successes and failures of simulated mesocyclone (MC) tracks using four different microphysics parameterization schemes (Table 1.) in a WoF setting.

Instead of using vertical vorticity to identify and track MCs (as in, e.g., Trapp and Weisman, 2003 and Schenkman et al., 2011), updraft helicity (UH; Kain et al., 2008, which used UH from 2 to 5 km AGL) is used because UH is the integral of the product of vertical vorticity and vertical velocity through a designated depth. The UH tracks are compared to each other and reality via estimated tornado point locations. Similar to hurricane track errors (Xue et al., 2013), UH track distance and timing errors are computed to assess model performance.

The numerical simulation methodology, including details about the observational data and model settings, are described in section 2. The verification methodology is described in section 3. Results of the numerical simulations and their verification are presented in section 4. Lastly, section 5 will provide a summary and discussion of the results, along with potential future work.

* *Corresponding author address:* Derek R. Stratman, The Univ. of Oklahoma, School of Meteorology, Norman, OK 73072; e-mail: stratman@ou.edu

2. SIMULATION METHODOLOGY

Since this experiment intends to explore the capabilities of the forecast system in a realistic setting, the numerical simulations use data from multiple observing platforms. Surface observations from NWS METAR and Oklahoma Mesonet stations and radial wind and reflectivity data from the WSR-88D [Dallas/Fort Worth (KFWS), Dodge City (KDDC), Frederick (KFDR), Tulsa (KINX), Twin Lakes (KTLX), Vance (KVNX), and Wichita (KICT)] and Collaborative Adaptive Sensing of the Atmosphere (CASA) IP-1 [Chickasha (KSAO), Cyril (KCYR), Lawton (KLWE), and Rush Springs (KRSP); see Fig. 1] radar networks (McLaughlin et al., 2009) are ingested into the initial analysis of the numerical simulations.

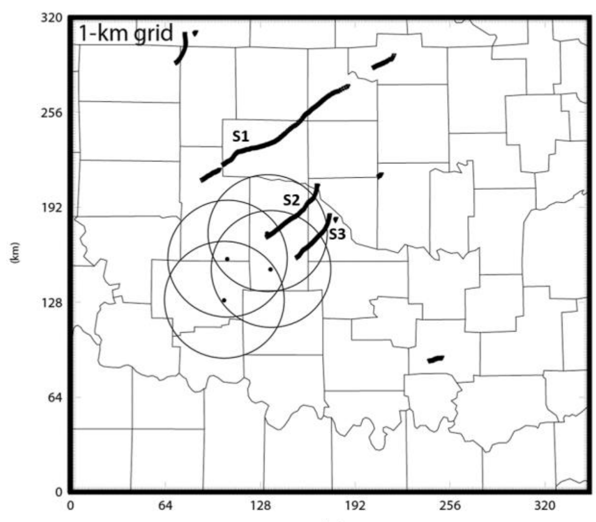

Figure 1. Domain of numerical simulations with CASA radar locations and 40-km range rings, estimated tornado points, and storm IDs.

Along with the observations, the 1800 UTC 12-km NAM (North American Mesoscale) model's 3-hour forecast (i.e., background field) is used in CAPS' Advanced Regional Prediction System's (ARPS; Xue et al., 2000; Xue et al., 2001; Xue et al., 2003) three-dimensional variational (3DVAR; Gao et al., 2004) and complex cloud analysis (Hu et al., 2006a,b) data assimilation process to produce an initial analysis on a 323x353-km domain with 1-km horizontal grid spacing (Fig. 1) and 53 vertically-stretched levels with a minimum dz of 20 m at the bottom. Three analysis passes with 20, 50, and 50 iterations, respectively, are used to produce the 3DVAR analysis through the minimization of the cost function. The surface in-situ data is implemented in the first and third passes, while the radar data is applied in the second and third passes. In addition, a 3D mass divergence constraint is utilized to couple the wind components together (Hu et al., 2006b).

After the 3DVAR analysis is produced, an ARPS simulation is integrated to produce forecasts out to 95 minutes. During the first 5 min, an incremental analysis update (IAU, Bloom et al., 1996) is performed by introducing increments every 20 s. The increments are applied to all fields except for vertical velocity and pressure since those two fields will quickly respond to the other fields and create a balanced state before the simulation proceeds on its own for the remaining 90 min.

During the integration of the ARPS simulation, a big and small time step of 2.0 s and 0.5 s, respectively, are employed in conjunction with the leapfrog time formulation. In addition, the 1800 UTC 12-km NAM forecasts are used for the lateral boundary conditions. Some other model details include: 4th-order momentum advection in both the horizontal and vertical directions, scalar advection using Zalesak's multi-dimensional version of flux-corrected transport (Zalesak, 1979), 1.5-order TKE closure based on Sun and Chang (1986), 4th-order computational mixing, Rayleigh damping beginning at 12-km AGL, National Aeronautics and Space Administration atmospheric radiation transfer parameterization, surface fluxes calculated from stability-dependent surface drag coefficients using predicted surface temperature and volumetric water content, and two-layer force-store soil model based on Noilhan and Planton (1989). The modeling process is summarized with a flow chart in Figure 2.

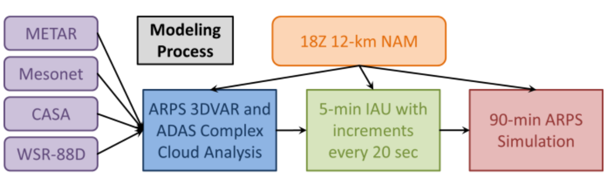

Figure 2. Flow chart of the modeling process used in this numerical simulation experiment.

Research experiments are done using four different microphysics parameterization schemes: Lin 3-ice microphysics scheme (Lin et al., 1983), Weather Research and Forecasting (WRF) single-moment 6-class microphysics scheme (Hong and Lim, 2006), Milbrandt and Yau (MY) single-moment bulk microphysics scheme, and MY double-moment bulk microphysics scheme (Milbrandt and Yau 2005a,b; Table 1).

ID	Microphysics Scheme
LIN3	Lin 3-ice microphysics
WSM6	WRF single-moment 6-class microphysics
MYSM	MY single-moment bulk microphysics
MYDM	MY double-moment bulk microphysics

Table 1. List of microphysics schemes used in the numerical simulations with their associated ID names.

In addition to microphysics diversity, simulations are run for three tornadic storms. The first storm (S1; storms depicted in Fig. 1) developed and stayed outside the CASA radar network and produced two tornadoes (Table 2), including the outbreak's only EF-5 tornado. The second and third storms (S2 and S3, respectively) developed in the CASA radar network and both produced EF-4 tornadoes, which dissipated before impacting the Oklahoma City metro area. To explore the capabilities of simulating MC tracks as related to the WoF concept, the ARPS simulations were initialized ~35 min before the first tornado touchdown for each storm.

Storm ID	Tornado Begin - End	ARPS Begin - End
S1	2031 Z - 2046 Z 2050 Z - 2235 Z	1955 Z - 2130 Z
S2	2206 Z - 2301 Z	2130 Z - 2305 Z
S3	2226 Z - 2305 Z 2302 Z - 2303 Z	2150 Z - 2325 Z

Table 2. List of storm ID names and associated tornado and ARPS-simulation forecast times.

3. VERIFICATION METHODOLOGY

To assess model performance, simulated MC tracks via the UH field are compared to each other and verified using estimated tornado points. The locations of the five tornadoes associated with the three storms of interest are estimated every minute based on NWS damage surveys, radar data, and high-resolution satellite data from Google Maps. Two adjacent layers of UH (i.e., 1–6 km and 0–1 km) are used for the verification of the simulations. These two layers represent simulated mid-level and low-level mesocyclones, respectively. As mentioned before, Kain et al. (2008) used UH from 2 to 5 km AGL to signify mid-level mesocyclones, but for this study, a deeper layer of UH is utilized to give more robust UH values by capturing more of the simulated mid-level MCs.

Since UH is a 2D field and not point data, a simple 2D object-based technique is utilized to find UH-weighted centers (analogous to mass-weighted centers), which will be verified against the estimated tornado points. A search radius of 10 grid points is used to isolate 1–6-km (0–1-km) UH maxima that are greater than or equal to 800 m^2 s^{-2} (60 m^2 s^{-2}) and their surrounding grid point values. A max UH value is considered a UH-center candidate if 6 out of 8 (4 out of 8) of the adjacent grid point values equals or exceeds 500 m^2 s^{-2} (40 m^2 s^{-2}). Once the UH-center candidates are determined, the UH-weighted center is computed using a radius of 5 grid points extending from the grid point with the max UH value.

With the UH-weighted center locations, an objective verification technique is used to find location and timing errors. First, distance errors are computed between the estimated tornado point locations and the nearest UH center locations at coincident times (referred to as same time for rest of paper). Second, distance and timing errors are calculated between the estimated tornado point locations and the nearest UH center locations at any occurrence time.

4. RESULTS

4.1 *Storm 1*

For S1, all of the 1–6-km UH (1-6UH) tracks exist north of the tornado tracks (Fig. 3a-d). LIN3's 1-6UH track is closest to the S1 tornado tracks, but the 1-6UH track extends further east than the other three simulations' 1-6UH tracks (Fig. 3a). MYDM's 1-6UH track is furthest from S1's estimated tornado tracks (Fig. 3d). Relative to WSM6's 1-6UH tracks, LIN3, MYSM, and MYDM all have 1-6UH tracks that are more narrow and intense. Similar results are found for the 0–1-km UH (0-1UH) tracks (Figs. 5a-d). However, the 0-1UH tracks are much narrower than the 1-6UH tracks, and most of the 0-1UH tracks are at least 1 km closer to the estimated tornado tracks.

For same-time distance errors, MYSM's average distance error for 1-6UH centers is between 1 km (i.e., MYDM) and almost 6 km (i.e., LIN3) closer than the other simulations' forecasts, but all simulations' 1-6UH centers are > 20 km downstream from the tornado points (Fig. 4a). When using 0-1UH, all simulations' UH centers are slightly closer to the tornado points than with using 1-6UH except for LIN3, which on average has 0-1UH centers almost 2 km further downstream than its 1-6UH centers (Fig. 6a).

For any-time distance and timing errors, LIN3's 1-6UH centers are on average > 1 km closer to the tornado points with distance errors mostly between 1 km and 5 km, but LIN3's 1-6UH centers are nearly 30 minutes too fast, which is over 4 minutes faster than the next fastest simulation (i.e., MYSM; Fig. 4d). MYDM's 1-6UH centers were the furthest from the tornado points, but on average, MYDM had the smallest time error. When using 0-1UH, the UH centers for all simulations were 1 to 3 km closer to the tornado points than the 1-6UH centers, but the average time errors were larger for all simulations except for MYSM (Fig. 6d). Once again, LIN3's 0-1UH centers were closest with an average distance error < 5 km, but LIN3's average timing error is > 7 min more than the timing errors from the other simulations.

Overall for S1, MYSM has the smallest same-time distance errors for both 1-6UH and 0-1UH, but the differences in same-time errors between WSM6, MYSM, and MYDM are smaller for 0-1UH than 1-6UH. Even though LIN3 is the fastest, its 1-6UH and 0-1UH centers have the smallest any-time distance errors, but due to being faster than the other simulations, LIN3 has the largest timing errors. On average, MYDM has the smallest timing errors, but the MYDM any-time distance errors are the largest.

4.2 *Storm 2*

Considering S2, all simulations produce 1-6UH tracks too soon and too far to the north of the estimated tornado tracks (Figs. 3e-h). LIN3 has the weakest 1-6UH track (Fig. 3e), while MYDM has the best defined 1-6UH track (Fig. 3h). Initially, all simulations have similar 0-1UH tracks, but every simulation weakens the 0-1UH track associated with S2 after the first 25 min or so into the forecast run (Figs. 5e-h).

Based on the average same-time distance errors, all simulations have 1-6UH centers that were > 35 km away (Figs. 4b). LIN3 has the largest same-time distance errors, while WSM6 has the smallest distance errors. However, WSM6's average same-time distance error for 1-6UH centers is misrepresented since several of the 1-6UH centers are associated with S3 and result in a lower distance error. Since there aren't many 0-1UH centers during the life-time of S2's tornado, no substantial conclusions can be made in relation to the same-time distance errors other than the simulations perform poorly for S2 (Fig. 6b).

For any-time distance and timing errors, most of the 1-6UH centers have distance errors > 16 km and timing errors > 30 min, excluding LIN3 (Fig. 4e). LIN3 appears to have a substantially smaller average timing error (i.e., ~8 min), but LIN3's errors are represented by only three 1-6UH centers, which is fewer than the other simulations. Similarly for 0-1UH, the simulations have 0-1UH centers > 16 km from the estimated tornado points and timing errors > 27 min except for MYSM, which has the same problem as LIN3 for the 1-6UH centers (Fig. 6e).

Generally for S2, the simulations exhibited a poor performance of forecasting UH tracks close to the estimated tornado points. This is disconcerting since S2 developed within the CASA radar network. However, S2 formed in between S1 and S3, so the case is convectively complex and thus inherently difficult to forecast. Also, simulations of this storm initialized after tornado development in the real-time configuration with LIN3 (not shown) were more successful.

4.3 *Storm 3*

Concerning S3, all simulations produce 1-6UH tracks very near the tornado tracks (Figs. 3i-l). As found for S2, LIN3 has the weakest 1-6UH track for S3 (Fig. 3i). MYSM's 1-6UH track almost perfectly matches the tornado track (Fig. 3k). WSM6 and MYDM both have 1-6UH tracks that are slightly to the north of the tornado track (Figs. 3j and 3l, respectively), but perhaps these tracks are closer to where the real mid-level MC was located relative to the tornado track than MYSM's 1-6UH track. Similar results are found for the 0-1UH tracks, which are marginally closer to the tornado track than the 1-6UH tracks (Figs. 5i-l).

The same-time distance errors reveal the simulations mostly have 1-6UH centers within 10 km of the estimated tornado points (Fig. 4c). LIN3 and WSM6 have average distance errors near 20 km, but each of those simulations have a single UH center about 40 km away from the closest same-time tornado point, which significantly skews the result. For 0-1UH, most UH centers are within 5 km of the tornado points (Fig. 6c). LIN3 has three 0-1UH centers that are substantially faster than the other simulations, with exception to one 0-1UH center for MYSM.

As depicted in Figure 4f, the simulations perform well with respect to 1-6UH's any-time distance and timing errors. All simulations have average any-time distance errors < 5 km and, except for LIN3, average timing errors < 8 min. In further evaluation, most of the 1-6UH centers are within 1 to 2 km of the estimated tornado points. The success of the simulations is highlighted even more for 0-1UH (Fig. 6f). The average timing errors for every simulation are a little worse than for 1-6UH, but the any-time distance errors are generally better. For example, MYSM has an average any-time distance error of about 0.71 km, as compared to 3.80 km for 1-6UH. In addition, the other three simulations for S3 have at least one 0-1UH center within 0.5 km of an estimated tornado point.

All things considered, the S3 simulations performed the best. Unlike for the S2 simulations, the CASA radar data may have improved the simulations with respect to small distance and timing errors, begging further investigation. Even though the UH centers still largely exist north of the tornado points, the northward bias is nearly zero.

5. SUMMARY AND DISCUSSION

On 24 May 2011, a well-forecasted tornado outbreak affected parts of central Oklahoma. For this study, three storms with violent tornadoes from this outbreak are used to evaluate the performance of a microphysically-diverse set of simulations. The evaluation of simulated MCs using the UH field against estimated tornado locations has proven to be an effective measure of model successes and failures. The simple, object-based verification technique applied in the evaluation process highlights these model successes and failures and helps define expected error bounds when utilizing microphysics diversity for the WoF ensemble concept (though any operational WoF will have a much larger ensemble size).

Some common themes emerge from the evaluations of the simulations. For example, UH centers tend to be too far north and too fast. This finding is not unique to this study as it has been found by other studies (e.g., Xue et al., 2014 and Potvin et al., 2014). Furthermore, 0-1UH centers are typically closer to the estimated tornado points than the 1-6UH centers. In regards to the WoF concept and ensemble spatial and temporal spread, the locations of UH tracks aren't substantially dissimilar among the tested simulations, but some potentially useful spread is evident in both the subjective and objective evaluations, especially after the first 15 min following the end of the 5-min IAU. Adjusting for the apparent northeastward bias may require more sophisticated post-processing.

As mentioned before, the simulations for S3 performed the best. Normally, this result wouldn't be surprising since S3 develops within the CASA radar network (e.g., Schenkman et al., 2011). However, S2 also develops within the CASA radar network, but the simulations of S2 here fail to produce UH centers in reasonable range of the estimated tornado points. Short of speculation, more research would need to be done before any potential conclusions could be made as to why the simulations struggled with S2 in this configuration. Except for UH centers existing a little to the north and substantially too far downstream from the tornado points, the simulations for S1 performed relatively well considering S1 remained outside the range of the CASA radar network.

Some potential future work might include the exploration of other variables (e.g., vertical vorticity, vertical wind, and horizontal wind) for verification using the simple object-based, center-tracking method developed for this study. Furthermore, application of this verification technique using the Storm Prediction Center's storm reports database instead of estimated tornado points could be used to verify a wide range of different severe storm episodes. Taking model verification one step further, the investigation into whether a model's analysis (e.g., 3DVAR/IAU analysis) can be used in place of estimated tornado points or storm reports for the verification of a model's forecast may be worth considering since any model field can then be verified with the same field from a real-time analysis.

Besides the verification aspect of this study, additional research could be directed at finding the optimal model initiation time needed to best forecast the occurrence of tornadogenesis and possibly mesocyclogenesis since this study only focused on initiation times ~35 min before tornadogenesis. Simulations initialized after tornadogenesis could also be performed to examine model performance of simulating MC maintenance and decay. Furthermore, simulations should be completed to specifically address the impact of using CASA radar data in the initial analysis on the simulated storms.

ACKNOWLEDGEMENTS

This work is supported by the National Science Foundation via CASA ERC grant EEC 03-13747 and related support provided by the University of Oklahoma (OU). Any opinions, findings, and conclusions or recommendations expressed in this material are those of the authors and do not necessarily reflect the views of the National Science Foundation. Some of the computing for this project was performed at the OU Supercomputing Center for Education & Research (OSCER) at OU. This work utilized data from the Oklahoma Mesonet provided by the Oklahoma Climatological Survey.

REFERENCES

Bloom, S. C., L. L. Takacs, A. M. da Silva, and D. Ledvina, 1996: Data Assimilation Using Incremental Analysis Updates. *Mon. Wea. Rev.*, 124, 1256–1271.

Gao, J., M. Xue, K. Brewster, and K. K. Droegemeier, 2004: A three-dimensional variational data analysis method with recursive filter for Doppler radars. *J. Atmos. Oceanic Tech.*, 21, 457-469.

Hong, S.-Y., and J.-O. J. Lim, 2006: The WRF single-moment 6-class microphysics scheme (WSM6). *J. Korean Meteor. Soc.*, 42, 129–151.

Hu, M., M. Xue, and K. Brewster, 2006: 3DVAR and Cloud Analysis with WSR-88D Level-II Data for the Prediction of the Fort Worth, Texas, Tornadic Thunderstorms. Part I: Cloud Analysis and Its Impact. *Mon. Wea. Rev.*, 134, 675–698.

Hu, M., M. Xue, J. Gao, and K. Brewster, 2006: 3DVAR and Cloud Analysis with WSR-88D Level-II Data for the Prediction of the Fort Worth, Texas, Tornadic Thunderstorms. Part II: Impact of Radial Velocity Analysis via 3DVAR. *Mon. Wea. Rev.*, 134, 699–721.

Kain, J. S., S. J. Weiss, D. R. Bright, M. E. Baldwin, J. J. Levit, G. W. Carbin, C. S. Schwartz, M. L. Weisman, K. K. Droegemeier, D. B. Weber, and K. W. Thomas, 2008: Some Practical Considerations Regarding Horizontal Resolution in the First Generation of Operational Convection-Allowing NWP. *Wea. Forecasting*, 23, 931–952.

Lin, Y.-L., R. D. Farley, and H. D. Orville, 1983: Bulk Parameterization of the Snow Field in a Cloud Model. *J. Climate Appl. Meteor.*, 22, 1065–1092.

McLaughlin, D., D. Pepyne, B. Philips, J. Kurose, M. Zink, E. Knapp, D. Westbrook, E. Lyons, A. Hopf, A. DeFonzo, R. Contreras, T. Djaferis, E. Insanic, S. Frasier, V. Chandrasekar, F. Junyent, N. Bharadwaj, Y. Liu, and Y. Wang, K. Droegemeier, M. Xue, J. Brotzge, F. Carr, K. Kloesel, K. Brewster, S. Cruz-Pol, and K. Hondl, 2009: Short-Wavelength Technology and the Potential for Distributed Networks of Small Radar Systems, *Bull. Amer. Meteor. Soc.*, 90, 1797-1817.

Milbrandt, J. A. and M. K. Yau, 2005: A Multimoment Bulk Microphysics Parameterization. Part I: Analysis of the Role of the Spectral Shape Parameter. *J. Atmos. Sci.*, 62, 3051–3064.

Milbrandt, J. A. and M. K. Yau, 2005: A Multimoment Bulk Microphysics Parameterization. Part II: A Proposed Three-Moment Closure and Scheme Description. *J. Atmos. Sci.*, 62, 3065–3081.

Noilhan, J. and S. Planton, 1989: A simple parameterization of land surface processes for meteorological models. *Mon. Wea. Rev.*, 117, 536-549.

Potvin, C. K., L. J. Wicker, M. M. French, and D. W. Burgess, 2014: Warn-on-Forecast Sensitivity Experiments with the 19 May 2013 Norman-Shawnee, OK, Tornadic Supercell. *Presentation at 27th Conf. on Severe Local Storms*, Madison, WI, 4 November 2014.

Schenkman A. D., M. Xue, A. Shapiro, K. Brewster, and J. Gao, 2011: Impact of CASA Radar and Oklahoma Mesonet Data Assimilation on the Analysis and Prediction of Tornadic Mesovortices in an MCS. *Mon. Wea. Rev.*, 139, 3422–3445.

Stensrud, D. J., L. J. Wicker, K. E. Kelleher, M. Xue, M. P. Foster, J. T. Schaefer, R. S. Schneider, S. G. Benjamin, S. S. Weygandt, J. T. Ferree, and J. P. Tuell, 2009: Convective-Scale Warn-on-Forecast System. *Bull. Amer. Meteor. Soc.*, 90, 1487–1499.

Stensrud, D. J., L. J. Wicker, M. Xue, D. T. Dawson, N. Yussouf, D. M. Wheatley, T. E. Thompson, N. A. Snook, T. M. Smith, A. D. Schenkman, C. K. Potvin,

E. R. Mansell, T. Lei, K. M. Kuhlman, Y. Jung, T. A. Jones, J. Gao, M. C. Coniglio, H. E. Brooks, K. A. Brewster, 2013: Progress and challenges with Warn-on-Forecast. *Atmos. Res.*, 123, 2-16.

Sun, W.-Y., and C.-Z. Chang, 1986: Diffusion model for a convective layer. Part I: numerical 864 simulation of convective boundary layer. *J. Climate App. Meteorol.*, 25, 1445–1453.

Trapp, R. J., and M. L. Weisman, 2003: Low-level mesovortices within squall lines and bow echoes. Part II: Their genesis and implications. *Mon. Wea. Rev.*, 131, 2804–2823.

Xue, M., K. K. Droegemeier, and V. Wong, 2000: The Advanced Regional Prediction System (ARPS) - A multiscale nonhydrostatic atmospheric simulation and prediction tool. Part I: Model dynamics and verification. *Meteor. Atmos. Physics.*, 75, 161-193.

Xue, M., K. K. Droegemeier, V. Wong, A. Shapiro, K. Brewster, F. Carr, D. Weber, Y. Liu, and D.-H. Wang, 2001: The Advanced Regional Prediction System (ARPS) - A multiscale nonhydrostatic atmospheric simulation and prediction tool. Part II: Model physics and applications. *Meteor. Atmos. Physics.*, 76, 134-165.

Xue, M., D.-H. Wang, J.-D. Gao, K. Brewster, and K. K. Droegemeier, 2003: The Advanced Regional Prediction System (ARPS), storm-scale numerical weather prediction and data assimilation. *Meteor. Atmos. Physics*, 82, 139-170.

Xue, M., J. Schleif, F. Kong, K. W. Thomas, Y. Wang, and K. Zhu, 2013: Track and Intensity Forecasting of Hurricanes: Impact of Convection-Permitting Resolution and Global Ensemble Kalman Filter Analysis on 2010 Atlantic Season Forecasts. *Wea. Forecasting*, 28, 1366–1384.

Xue, M., M. Hu, and A. D. Schenkman, 2014: Numerical Prediction of the 8 May 2003 Oklahoma City Tornadic Supercell and Embedded Tornado Using ARPS with the Assimilation of WSR-88D Data. *Wea. Forecasting*, 29, 39–62.

Zalesak, S. T., 1979: Fully Multidimensional Flux-Corrected Transport Algorithms for Fluids. *J. Comput. Phys.*, 31, 335–362.

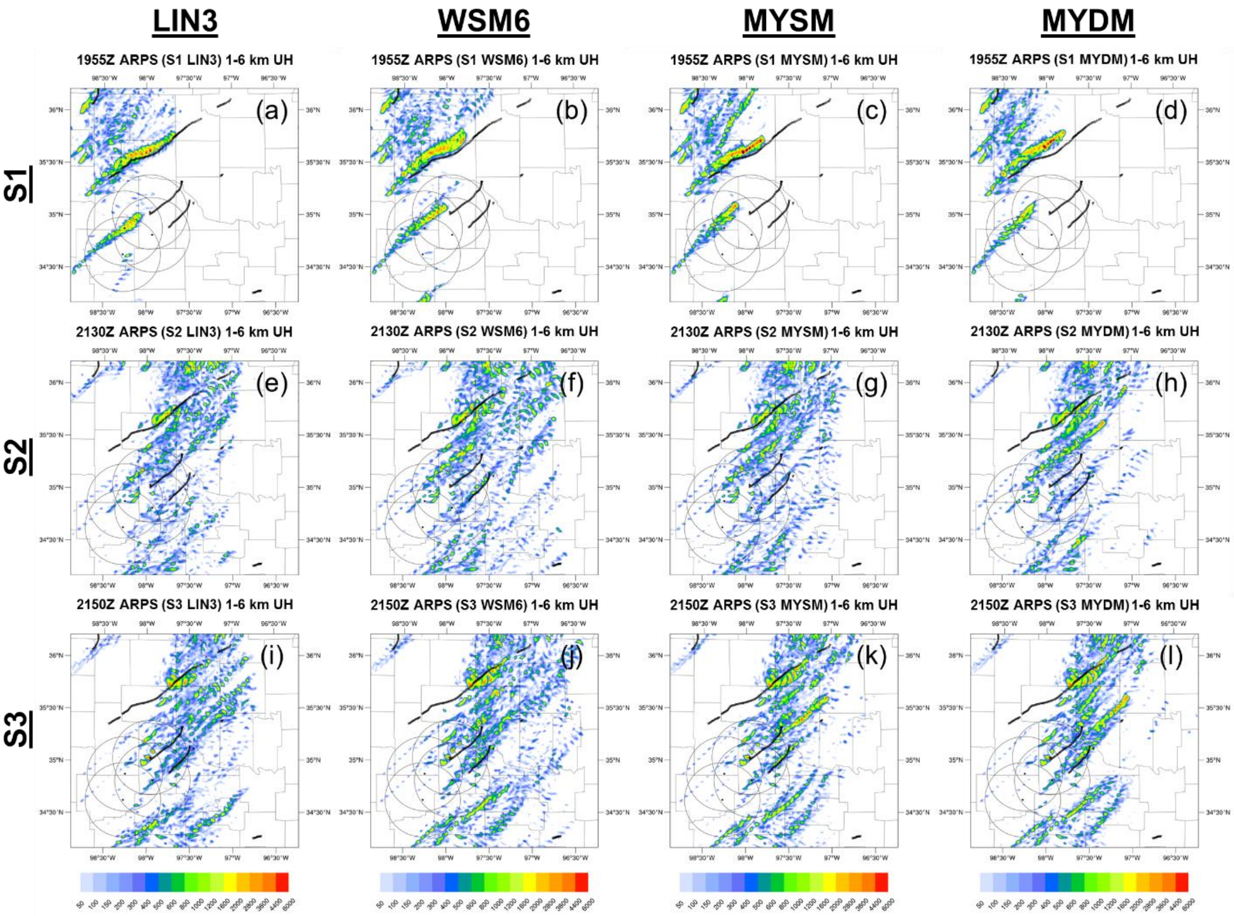

Figure 3. Plots of maximum 1–6-km UH from forecasts every 5 min for each of the simulations. Small black triangles represent estimated tornado points every 1 min. Small black-filled circles represent the locations of the CASA radars, and the larger black circles indicate the 40-km range of the individual CASA radars.

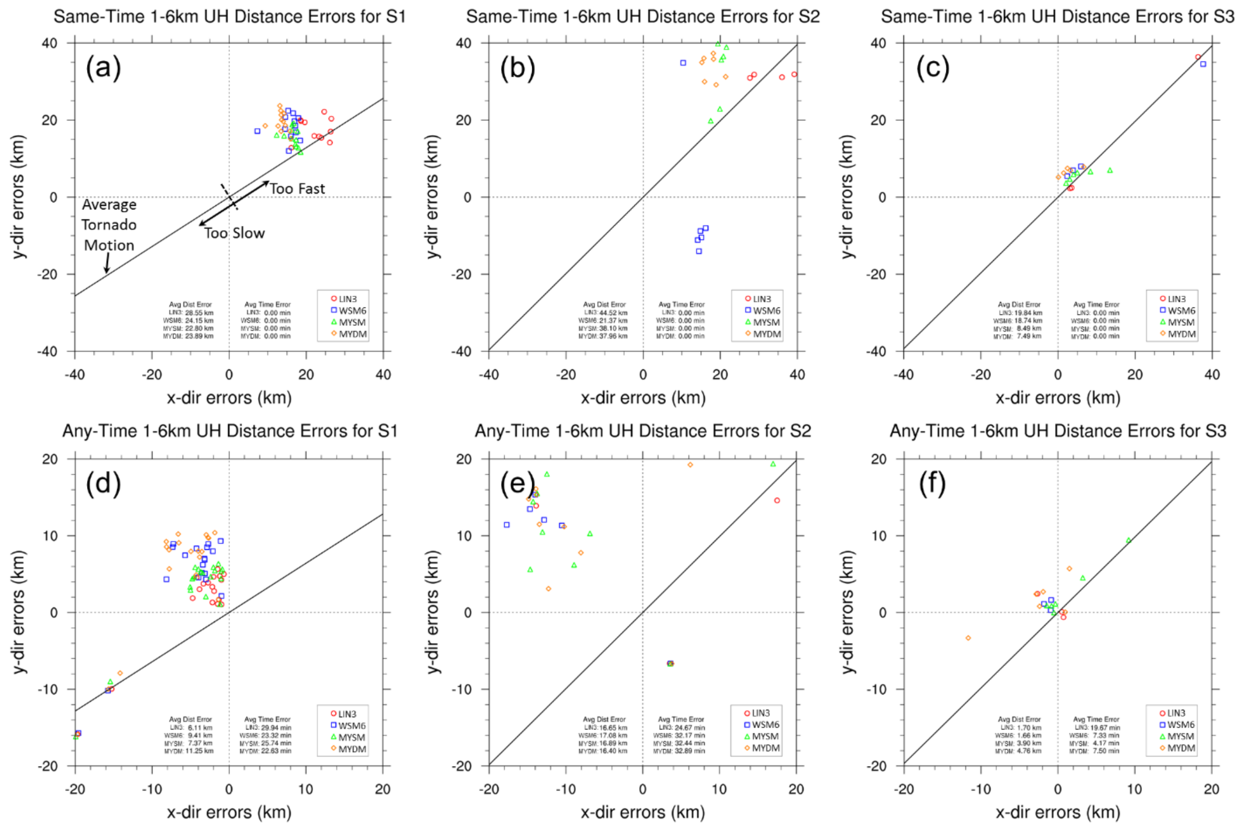

Figure 4. Same-time distance errors between 1–6-km UH centers and estimated tornado points for (a) S1, (b) S2, and (c) S3. Any-time distance and time errors between 1–6-km UH centers and estimated tornado points for (d) S1, (e) S2, and (f) S3. For reference, diagonal solid black lines represent the average tornado motions for each storm.

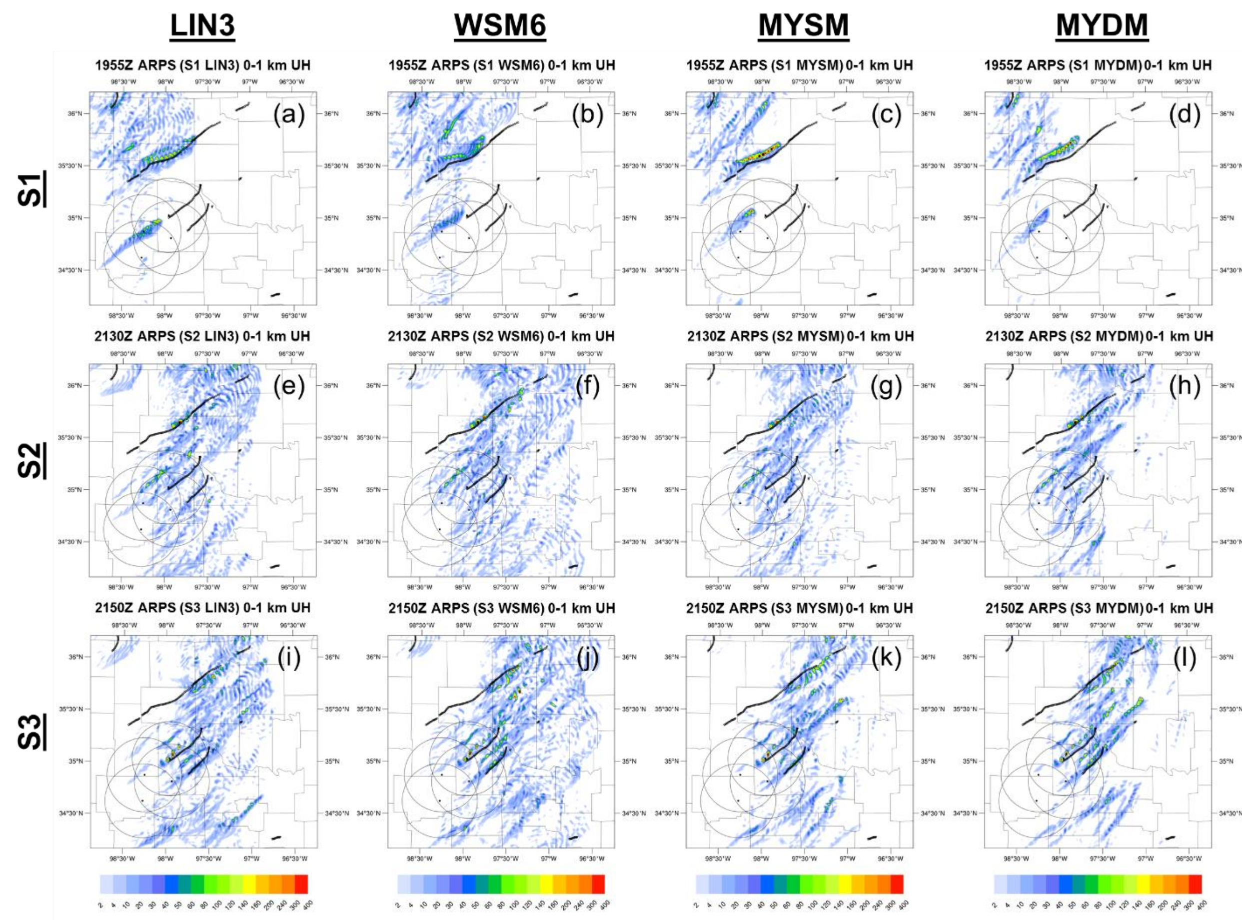

Figure 5. Same as in Fig. 3, but for 0–1-km UH instead.

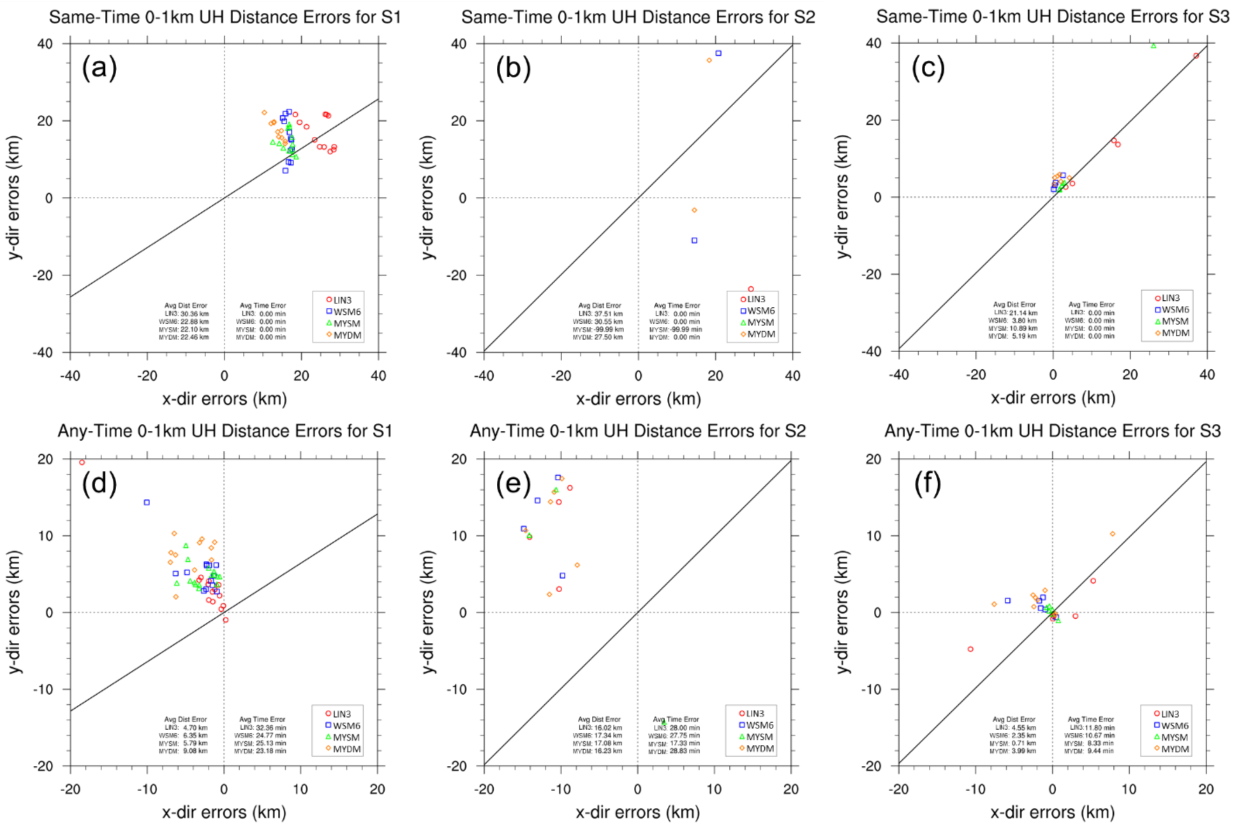

Figure 6. Same as in Fig. 4, but for 0–1-km UH instead.